

# Hydrodynamic instabilities in a highly radiative environment

Cite as: Phys. Plasmas **29**, 072106 (2022); <https://doi.org/10.1063/5.0089994>

Submitted: 02 March 2022 • Accepted: 26 June 2022 • Published Online: 14 July 2022

 G. Rigon, B. Albertazzi, P. Mabey, et al.



View Online



Export Citation



CrossMark

## ARTICLES YOU MAY BE INTERESTED IN

[Rayleigh–Taylor and Richtmyer–Meshkov instabilities in the presence of an inclined magnetic field](#)

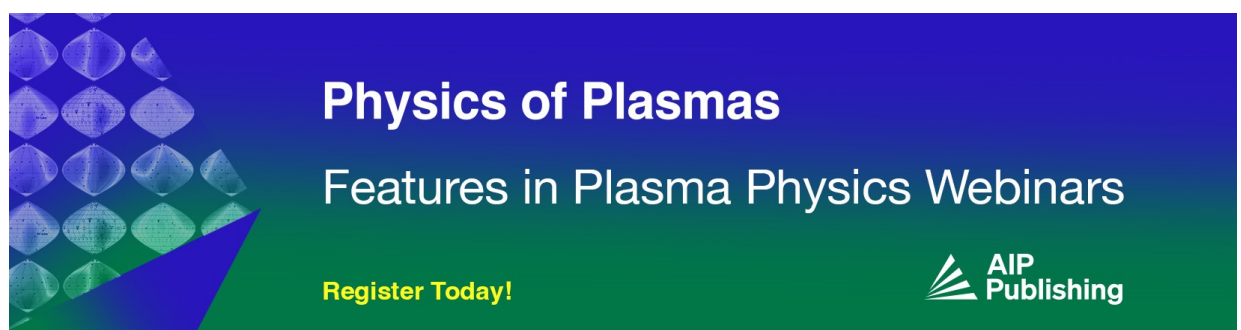
Phys. Plasmas **29**, 072104 (2022); <https://doi.org/10.1063/5.0091639>

[Self-generated magnetic field in ablative Rayleigh–Taylor instability](#)

Phys. Plasmas **29**, 072702 (2022); <https://doi.org/10.1063/5.0092234>


[Role of self-generated magnetic fields in the inertial fusion ignition threshold](#)

Phys. Plasmas **29**, 072701 (2022); <https://doi.org/10.1063/5.0091529>



**Physics of Plasmas**  
Features in Plasma Physics Webinars

Register Today!



# Hydrodynamic instabilities in a highly radiative environment

Cite as: Phys. Plasmas **29**, 072106 (2022); doi: 10.1063/5.0089994

Submitted: 2 March 2022 · Accepted: 26 June 2022 ·

Published Online: 14 July 2022



View Online



Export Citation



CrossMark

G. Rigon,<sup>1,2,a)</sup> B. Albertazzi,<sup>1</sup> P. Mabey,<sup>1,3</sup> Th. Michel,<sup>1</sup> P. Barroso,<sup>4</sup> A. Faenov,<sup>5</sup> R. Kumar,<sup>6</sup> C. Michaut,<sup>7</sup> T. Pikuz,<sup>8</sup> Y. Sakawa,<sup>6</sup> T. Sano,<sup>6</sup> H. Shimogawara,<sup>6</sup> S. Tamatani,<sup>6</sup> A. Casner,<sup>9</sup> and M. Koenig<sup>1,10</sup>

## AFFILIATIONS

<sup>1</sup>LULI, CNRS, CEA, Ecole Polytechnique, UPMC, Univ Paris 06: Sorbonne Universites, Institut Polytechnique de Paris, F-91128 Palaiseau Cedex, France

<sup>2</sup>JSPS International Research Fellow, Graduate School of Science, Nagoya University, Furo-cho, Chikusa-ku, Nagoya 464-8602, Japan

<sup>3</sup>Department of Physics, Freie Universität Berlin, Arnimallee 14, 14195 Berlin, Germany

<sup>4</sup>GEPI, Observatoire de Paris, PSL University, CNRS, 77 Avenue Denfert Rochereau, 75014 Paris, France

<sup>5</sup>Joint Institute of High Temperatures, Russian Academy of Science, Moscow 125412, Russia

<sup>6</sup>Institute of Laser Engineering, Osaka University, Osaka 565-0871, Japan

<sup>7</sup>Observatoire de la Côte d'Azur, CNRS, Laboratoire Lagrange, Université Côte d'Azur, Nice 06304, France

<sup>8</sup>Institute for Open and Transdisciplinary Research Initiatives, Osaka University, Osaka 565-0871, Japan

<sup>9</sup>CEA-CESTA, 15 Avenue des Sablières, CS 60001, 33116 Le Barp CEDEX, France

<sup>10</sup>Graduate School of Engineering, Osaka University, Osaka 565-0871, Japan

<sup>a)</sup>Author to whom correspondence should be addressed: [gabriel.rigon@nagoya-u.jp](mailto:gabriel.rigon@nagoya-u.jp)

## ABSTRACT

In this paper, we present the effects of a radiative shock (RS) on the morphology of jet-like objects subjected to hydrodynamic instabilities. To this end, we used an experimental platform developed to create RSs on high energy laser facilities such as LULI2000 and GEKKO XII. Here, we employed modulated targets to initiate Richtmyer–Meshkov and Rayleigh–Taylor instability (RTI) growth in the presence of an RS. The RS is obtained by generating a strong shock in a dense pusher that expands into a low-density xenon gas. With our design, only a limited RTI growth occurs in the absence of radiative effects. A strongly radiative shock has opposite effects on RTI growth. While its deceleration enhances the instability growth, the produced radiations tend to stabilize the interfaces. Our indirect experimental observations suggest a lower instability growth despite the interface deceleration. In addition, the jets, produced during the experiment, are relevant to astrophysical structures such as Herbig–Haro objects or other radiatively cooling jets.

Published under an exclusive license by AIP Publishing. <https://doi.org/10.1063/5.0089994>

## I. INTRODUCTION

In high energy density physics (HEDP), radiation has an important impact on the properties of fluids and flows.<sup>1</sup> One of the effects of radiation is the modification of the structure of a shock both upstream with the generation of a precursor and downstream. A radiative shock (RS) happens when the temperature of the shock front is high enough to induce a non-negligible radiative flux from visible to x rays. The photons, thus produced, can be absorbed by the surrounding medium. Upstream from the shock, the thermodynamic parameters may be modified (rise in the temperature, ionization, etc.) forming what is known as a precursor.<sup>2</sup> In particular, a radiative precursor can lead to a smooth transition of the temperature from the upstream medium to

the shocked medium. Radiative losses at the shock front can also lead to the deceleration of the RS as soon as they are no longer negligible.<sup>3</sup> Both direct modification of the shock structure and its deceleration shape the dynamics of a physical system in the presence of radiations.

In HEDP, RSs influence numerous systems. In astrophysics, they intervene in various situations: radiative cooling in Herbig Haro jets,<sup>4</sup> polar objects,<sup>5–7</sup> the circumstellar ring of SN 1987A,<sup>3,8,9</sup> etc. In inertial confinement fusion (ICF), the converging shock becomes radiative after its reflection.<sup>10</sup> All these systems are also influenced by hydrodynamic instabilities. These instabilities naturally appear in most flows and can be coupled with radiative effects. This coupling applied to the Rayleigh–Taylor instability (RTI), which grows at the interface

between fluids when the gradient of density opposes the gradient of pressure, and to the Richtmyer–Meshkov instability (RMI), the result of a shock crossing an interface.<sup>11,12</sup> Both of these instabilities can not only be found in ICF: in the ablative phase<sup>13–18</sup> (interaction between the drive and the target) but also in a decelerating phase during final capsule convergence.<sup>19</sup> These two phases also present significant radiative flux. Since the growth of the RTI is modified in the ablative phase,<sup>20,21</sup> it seems natural to consider interactions between radiative phenomena and instabilities. In that context, a tentative study of the RTI growth in the presence of radiative flux was performed by Kuranz *et al.*<sup>22</sup> in an indirect drive configuration.

Here, we wish to go further and study the growth of hydrodynamic instabilities (RTI and RMI) following a radiative shock and the possibility of RTI growth as a consequence of highly radiative effects. Contrary to the above-mentioned experimental study, in our experiment, the radiative flux is produced *in situ* by the shock, and the RTI growth is weak in the absence of strong radiative effects. Such a situation arises in the presence of a steady shock, as the unstable interface does not decelerate. In such a case, the growth rate of the RTI,  $n_0$ , is null as no inertial-pseudo force,  $g$ , exists in the reference frame of the interface. Indeed, in a first-order approximation,  $n_0$  equals  $\sqrt{A_n k g}$  with  $A_n = (\rho_1 - \rho_2)/(\rho_1 + \rho_2)$  being the Atwood number and  $k$  being the wavenumber of the perturbation. Conversely, in the presence of a strongly radiative shock, which decelerates,<sup>3</sup> RTI should develop. Such a situation can be related to astrophysical jets and their radiative cooling.<sup>4</sup> Yet, the radiation produced by such shock may also have the opposite effect on the hydrodynamic instabilities. Indeed, it is well known that the presence of radiation stabilizes RT unstable interfaces by ablating them.<sup>20,22,23</sup> A similar stabilization effect should also modify the RMI growth. In addition to this, a strong shock deceleration can lead to closer proximity between the shock and interface. The resulting pressure gradient across the interface also impacts the instability growth.<sup>24,25</sup> This article presents an experimental approach to study this situation.

In Sec. II, we present the different experimental setups used in this study. In Sec. III, we focus on the experimental results that highlight, in a first step, the presence of a shock, and in Sec. II, the development of both RTI and RMI. In Sec. IV, we discuss the global jet morphology in regard to the presence of a radiative shock and instability development. This section builds on the analogy between the morphology of our experimental jets and of astrophysical jets.

## II. EXPERIMENTAL SETUP

In HEDP, one of the main techniques to create a radiative shock in a controlled environment is to use a high power laser.<sup>26–30</sup> The experiments described in this work, therefore, took place at the GEKKO XII laser facility (ILE, Osaka University, Japan) and the LULI2000 laser facility (LULI, Ecole Polytechnique, France).

To experimentally study the effect of a radiative shock and its deceleration on the development of RTI, it is necessary to create a situation where the RTI growth should be faint in the absence of radiations. To this end, we need to create a system where there is almost no deceleration,  $g \simeq 0 \mu\text{m ns}^{-2}$ . In order to do so, we produced and propagated a plasma flow in a low-pressure gas, which will offer nearly no resistance to the plasma motion. Depending on the nature of the gas: low (helium—He) or high (xenon—Xe) atomic number, the shock, which precedes the flow, will be either classical or radiative.<sup>3</sup> When the radiative energy becomes over few percent, of the total energy, the shock will decelerate.<sup>3</sup>

Accordingly, we used the gas cells developed at the LULI laboratory to perform laser experiments, where a piston generates a shock in a gas. The gas cells, we used, are designed with up to three observation axes (see Fig. 1). As in our previous experiments,<sup>3,31</sup> the laser irradiates a solid target blocking the entrance of the gas cell. This target is composed of three layers: a  $10 \mu\text{m}$  parylene ablator, a  $1 \mu\text{m}$  gold shield, a  $40 \mu\text{m}$  modulated brominated plastic pusher. The gas cell is filled with a low density gas ( $5.4 \times 10^{-5} \text{ g cm}^{-3}$ ) either He ( $\sim 330 \text{ mbar}$ ), a non-radiative medium, or Xe ( $\sim 10 \text{ mbar}$ ) a radiative medium. The ablation of the ablator by the laser generates a shock wave that breaks out into the gas setting the interface (pusher-gas) in motion.

Depending on the laser facility, GEKKO XII or LULI2000, the reachable laser conditions differ. At GEKKO XII, we employed the superposition of nine laser beams (at  $351 \text{ nm}$  wavelength) resulting in a  $600 \mu\text{m}$  diameter flat top focal spot (kinoform phase plate), an intensity of  $7.1 \times 10^{14} \text{ W cm}^{-2}$  with a  $\sim 0.5 \text{ ns}$  Gaussian pulse, for a total energy of  $\sim 1080 \text{ J}$ . At LULI2000, we used the nano2000 laser (at  $527 \text{ nm}$  wavelength) to create a  $\sim 470 \mu\text{m}$  diameter near flat (hybrid phase plate) focal spot, in a  $1.5 \text{ ns}$  square pulse for an intensity of  $1.9 \times 10^{14} \text{ W cm}^{-2}$ , and a total energy of  $\sim 500 \text{ J}$ . The pressure resulting from the ablation (theoretically  $> 25 \text{ Mbar}$ <sup>32–34</sup>) and, consequently, the post-shock pressure are much greater than the initial gas pressure ( $10 \text{ mbar}$  of Xe or  $330 \text{ mbar}$  of He), which as a result is negligible.

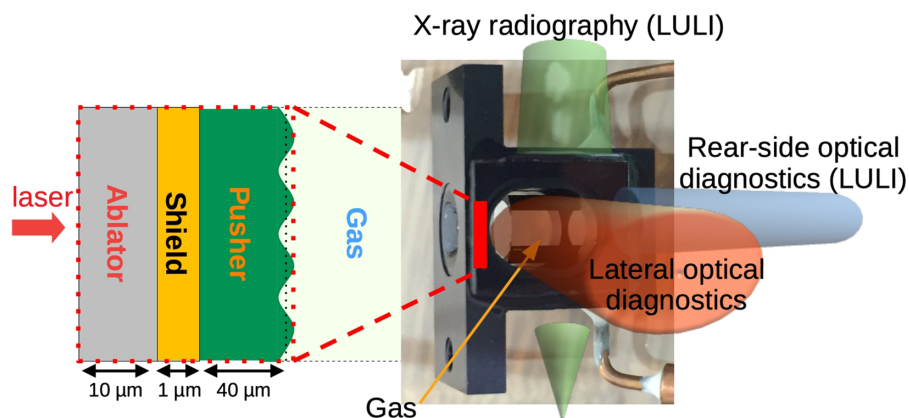


**FIG. 1.** Experimental setup. A multilayer modulated target designed for a controlled RTI growth is ablated by a high energy laser. As a result, the pusher will expand into a gas, which is contained in a cell. The resulting situation is diagnosed along three different axes.

These pressure conditions correspond to the strong shock. Thus, the dynamics of the shock and the expanding plasma should be the same in Xe and He from a purely hydrodynamic point of view. One might wonder about the effects of the difference in sound speed, which results from the difference in gas pressure. However, such effects are negligible in our experiment when considering the presence of a radiative precursor in Xe. According to our simulation (see below), the pre-shock sound speed, which should be the largest in He when considering the difference in pressure, is actually larger in Xe, because of the precursor.

Our targets are specially designed for the study of RMI and RTI. In particular, the pre-imposed modulation of the pusher serves as a seed for the instabilities. In these experiments, a single sine wave modulation with 120  $\mu\text{m}$  wavelength and 10  $\mu\text{m}$  amplitude was machined on the pusher. This ensures that the growing perturbation is not random, neither due to the local variation of laser intensity (speckles) nor to variation in the target quality (material roughness). Thus, the data obtained on different laser shots can be compared to each other, leading to a reproducible experiment.

To follow the development of the instabilities, we implemented multiple diagnostics along three lines of sight depending on the laser facility used (see Fig. 1). In the horizontal plane, we implemented all the diagnostics using visible light, which we will refer to as optical diagnostics. These are based on different techniques such as optical pyrometry, interferometry, shadowgraphy, and Schlieren. All of them were streaked (1D spatial with time evolution) and gated (2D spatial resolved in time—integrated over 0.125 ns). In addition to these optical diagnostics, we used x-ray radiography in a down-up geometry on LULI2000. The x-ray source was produced by focusing the pico2000 laser beam (55 J, 10 ps) on a 25  $\mu\text{m}$ -diameter titanium wire. The resulting snapshots present a magnification of  $\sim 38$  for a spatial resolution of  $\sim 25 \mu\text{m}$ .<sup>31</sup>

### III. EXPERIMENTAL RESULTS

#### A. Radiative effects

Our study concerns radiative effects on hydrodynamic instabilities, so the presence of radiation should first be ensured. However, depending on the facility (GEKKO XII or LULI2000), a major difference in the laser intensity exists. This implies a disparity in the level of the radiative effects that can be achieved.

As a first step, we establish the presence or absence of radiative precursors depending on the nature of the gas using interferometry techniques. Indeed, this diagnostic allows us to observe the variation of electron density, and consequently the ionization induced by a precursor. As can be seen in Fig. 2, the interference pattern in the upstream medium differs between the He and Xe cases. The fringes are shifted in the Xe case, highlighting a variation in the electron density in the unshocked region. Supposing our system has a nearly cylindrical geometry (axial symmetry), we determined the electron density map in the xenon gas using inverse Abel transformation. In Xe, the preshocked gas has an electron density of  $\sim 2 \times 10^{18} \text{ cm}^{-3}$ . This corresponds to an ionization of  $\sim 8$  given the initial xenon density ( $\sim 2.5 \times 10^{17} \text{ cm}^{-3}$ ). This electron density and ionization testify the presence of a strong radiative precursor. In helium, the fringes remain unperturbed, showing the absence of an ionization front upstream from the shock.

The observation of the self-emission of the plasma, using two-dimensional pyrometry diagnostics, also allows us to ascertain the existence of a radiative precursor in the Xe gas (see Fig. 3). Such emission is due to the shock temperature (grey body emission) and electronic processes (electron transition). Thus, self-emission is significant where internal energy is high, for instance, at the shock front, in the shocked gas, but also to a lower extent in the radiative precursor. In Fig. 3, we can see the high emission of the shocked gas and shock front, which form the first arc (both in He and Xe). Here, we can also see a second arc, highly similar to the first one in terms of morphology. This second arc is an artifact of our diagnostic, produced by a parasitic reflection in the optical path (double reflection inside a beam splitter). In the Xe case (B), a low emission third arc precedes the shock front, as highlighted by the line-out (C). This third arc corresponds to the radiative precursor, which is present only in Xe.

These results are also supported by a theoretical approach, which also allows us to infer the radiative nature of the shocks. According to models developed in previous articles,<sup>3,35</sup> there is a shock velocity threshold, above which radiative effects start to become non-negligible. A higher shock velocity results in a higher post-shock temperature. In turn, this higher temperature has consequences on the balances of energy density and energy flux, as radiative flux and energy increase faster with the temperature than their thermal counterpart. As a consequence, a shock velocity threshold exists. It depends on the gas density and composition and uses an estimate of the shock

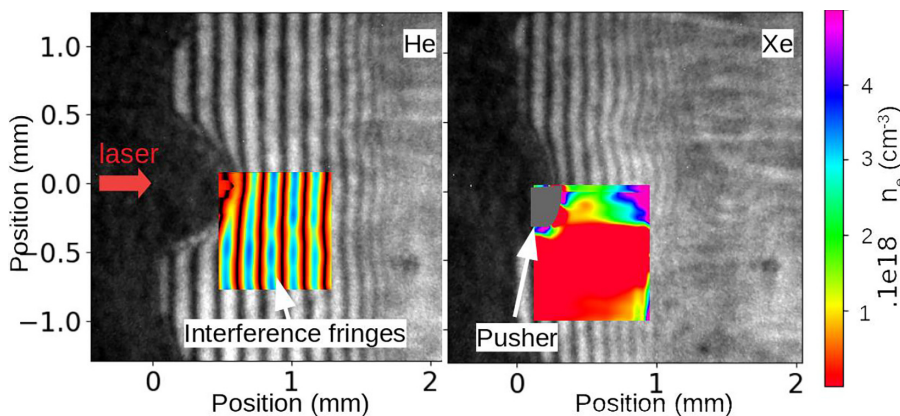
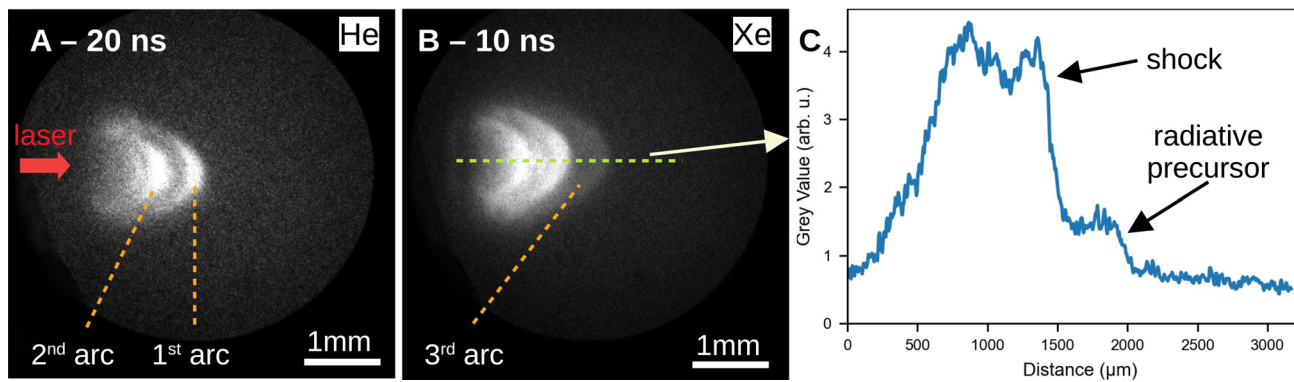


FIG. 2. Interferometry images obtained 8 ns after laser shot on GEKKO XII. The interference fringes remain straight in He. They are slightly curved in Xe, which indicates a change in the electron density due to the radiative precursor. The electron density map deduced from the fringe pattern is shown on half of the Xe image.





**FIG. 3.** Comparison of the self-emission of the plasma in both He (a) and Xe (b) as obtained on LULI2000. On these pyrometry images, two highly luminous parallel arcs appear. The second one is an artifact. The third arc, present in Xe only, corresponds to the radiative precursor. (c) Line-out on the propagation axis in the Xe case [green dashes on (b)].

temperature taking into account the gas ionization as well as the radiative energy and flux. (Older models based on the Boltzmann and Mihalas numbers did not take into account the ionization.) Accordingly, we calculate a critical velocity of  $24 \text{ km s}^{-1}$  in Xe and  $383 \text{ km s}^{-1}$  in He. We compare these critical velocities to the shock velocity measured experimentally using optical streaked diagnostics. We should mention that the initial shock velocity (right after the shock breaks out in the gas) does not depend on the type of gas used as it is only linked to the initial ablation pressure. We measured a respective shock velocity of  $45 \pm 5$  and  $100 \pm 10 \text{ km s}^{-1}$  on LULI2000 and GEKKO XII experiments. It can be deduced that the radiative effects are negligible in He; therefore, the propagation of the shock is purely hydrodynamic (reference), whereas the radiative effects are present in Xe. Moreover, the shock is only weakly radiative on LULI2000 and more strongly on GEKKO XII.

These stronger radiative effects on GEKKO XII are associated with a slight deceleration of the shock and following interface. This deceleration is too low to be temporally measured with the streaked diagnostic. We can, however, estimate its value based on the gap in shock position between He and Xe at late times (40 ns). As the gap we observed is of the order of  $100 \mu\text{m}$  on a 4 mm jet, we can estimate a deceleration of the order of  $0.1 \mu\text{m ns}^{-2}$ . These values are subject to caution as they ultimately depend on the laser intensity (and the resulting shock velocity), which varies from shot to shot.

In conclusion, we have fulfilled the fundamental conditions to study hydrodynamic instabilities in a radiative environment using xenon, the helium case being a reference.

## B. Instabilities and morphology

Now, we will focus on the development of hydrodynamic instabilities. To this end, we mainly consider the 2D experimental snapshots, which we compare to corresponding simulations.

We performed simulations using the FLASH4 code (v. 4.2.2), an Eulerian code including an HEDP module (laser-matter interaction, multi-group radiation, etc.) developed at the Flash Center (Chicago University).<sup>36–38</sup> The simulations were performed in a 2D Cartesian geometry over a  $1400 \times 2100 \mu\text{m}$  domain divided in  $2 \times 3$  main blocks refined by a sixth order adaptive refinement scheme

(PARAMESH 4dev) in sub-blocks containing  $16 \times 16$  cells for a maximal resolution of  $1.4 \mu\text{m}$ . The simulations were initialized with the same geometry as the experiment, except for the gold layer, too thin to be resolved. They were solved using a hydrodynamic solver, including radiation transport and multiple temperatures (ion, electron, radiation). We used an “hllc” Riemann solver, second order spatial reconstruction, and “mc” slope limiter. Tabulated equations of states (EoS) and opacities were employed for each target component. EoS were produced using IONMIX, whereas the opacities were calculated over 40 radiative groups using PROPACEOS. The laser intensity in the simulations was adapted to reproduce the shock motion during the early phase (the same shock/interface motion after shock’s break-out).

While the simulations allow us to qualitatively understand most of our experimental results, the uncertainty in our observations does not allow us to validate with certainty our simulations. The simulations recreate the early dynamic and global morphology of our expanding pusher and shock. However, our simulations are based on numerous approximations (2D, tabulated EoS, opacities, etc.), and they employ a modified laser intensity to recreate the initial expansion dynamic. As such, the simulated values, while showing the correct variations, are questionable. For instance, our simulations predict a radiative precursor in Xe and none in He. The simulated radiative precursor has an electron temperature,  $T_e$ , between  $3 \times 10^4$  and  $5.5 \times 10^4 \text{ K}$ , and an electron density,  $n_e$ , between  $6 \times 10^{17}$  and  $\sim 1 \times 10^{18} \text{ cm}^{-3}$  on LULI2000 and slightly higher value on GEKKO XII:  $T_e \sim 6.6 \times 10^4 \text{ K}$  and  $n_e \sim 1.2 \times 10^{18} \text{ cm}^{-3}$ . These values are slightly lower than what our experimental results suggest. This difference is due to the uncertainty of our observations and analysis and to the approximation of the simulations. Indeed, the electron temperature and electron density of the precursor depend on the opacity tables used for Xe and on the laser intensity. So, while the qualitative analysis (the presence of a radiative precursor) is not affected, the quantitative analysis (electron temperature and density) might be wrong.

The first instability, which grows in our experiment, is the RMI. This instability is a consequence of the shock crossing the modulated interface. This is observed with our rear side streaked optical pyrometry (SOP) (see Fig. 4). The SOP shows the temporal evolution of the self-emission of the target rear side. The emission starts after the shock breaks out of the gold layer. Before that time the visible light,

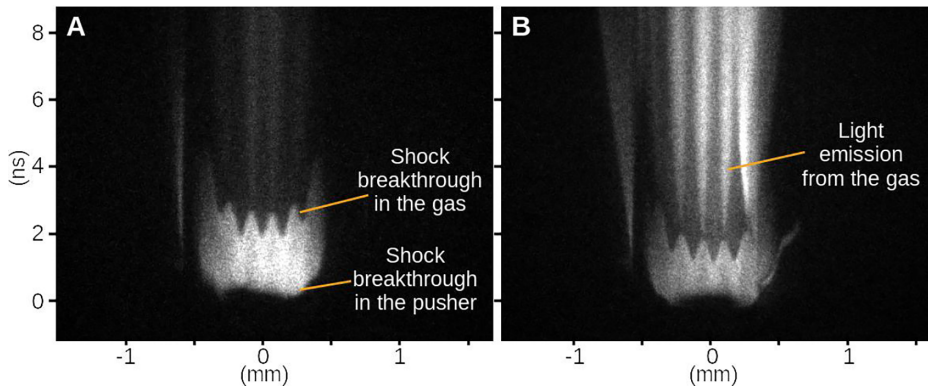


**FIG. 4.** Result of the rear side SOP (LULI2000) both in helium (a) and xenon (b). The emission is produced first in the pusher and then at the shock front. It is more important in xenon than in helium.

emitted at the shock front, is absorbed by the gold layer. After breakout, only the gas and the pusher contribute to the absorption. Both are transparent to the visible light, thus self-emission is observed. When the shock is then transmitted to the gas, the light emission becomes lower. The lower emission is partly due to the lower density of the gas in comparison to the pusher. Looking at the lateral position, the shock breakout occurs at different times due to the pusher modulation. (It happens later on the initial spike's axis.) As a result, a modulation appears on the streaked self-emission images. After the brightness decreases in the gas, the self-emission increases again in localized zones, along the axes of the initial modulation spikes. These axes also correspond to the axes of the bubbles of the developing instability, since the RMI leads to an inversion of the modulation in this configuration. So the emission in the gas is mostly produced in the axis of the RTI/RMI bubbles.

As can be seen with the Xe simulation results shown in Fig. 5, the shocked gas accumulates between the spikes of the instability, where it becomes hot (red spots between 9.5 and 12 ns). This pinched hot gas emits the light, which we observe. As the shock propagates, it flattens out. (The modulations of the shock disappear.) This results in the lateral diffusion of the hot spots, which are no longer constrained. This phenomenon can be seen in the last simulation panel (16 ns), where all the hot spots have nearly disappeared and have been replaced by a high-temperature line that spans laterally across the whole shock front.

This broadening can also be observed in experiment with the backside SOP (Fig. 4). Indeed, the localized emissions in the gas broaden with time and tend to form a uniform emission front. This observation is an indirect hint of the instability development. A similar phenomenon of hot spot formation and diffusion can be observed in He. However, they possess a lower intensity compared to the ones in Xe, and they diffuse quickly. According to our simulations, the electron temperature of these hot spots,  $\sim 3 \times 10^4$  K, is much lower than the one in Xe,  $\sim 2.5 \times 10^5$  K. This lower temperature explains the lower emission observed with the rear SOP, Fig. 4(a). Because of their low temperature, which is of the order of the post-shock temperature ( $\sim 2.5 \times 10^4$  K), the hot spot quickly thermalizes. This thermalization is also quickened by the morphology of the interface in He. Contrary to the large RTI spikes that appear in Xe, the RTI spikes in He are thinner and longer in He. The resulting larger space between spikes allows convective motions that can contribute to the thermalization. However, this short analysis is only based on our simulations, as we did not manage to directly observe the instability in experiments. The rear side SOP results alone are too thin evidence to support the simulation results on RTI morphology.

More direct observations of the instabilities can be obtained using x-ray radiography. Figure 6 shows such radiography (a) and (b) as well as a synthetic one obtained by post-processing the FLASH4

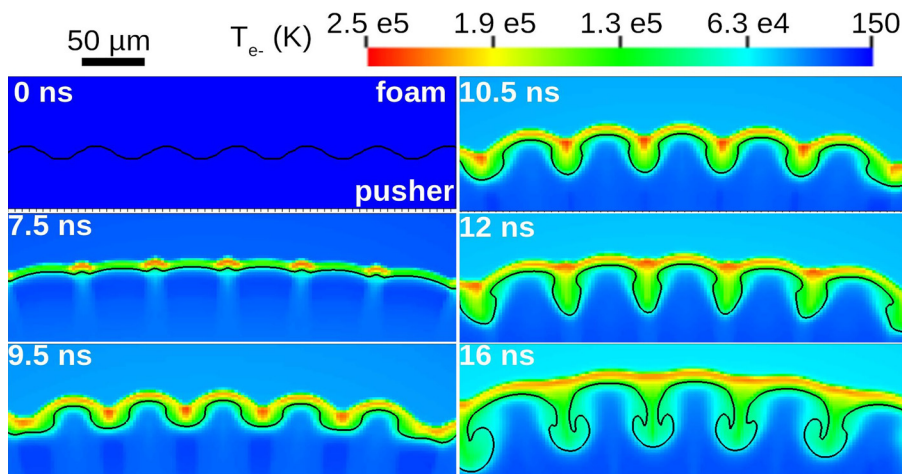


**FIG. 5.** Evolution of the electron temperature along the interface according to FLASH simulations of the LULI2000 experiment in Xe. Here, the interface is displayed as a black line, and the electron temperature is depicted in a pseudo-colour map.

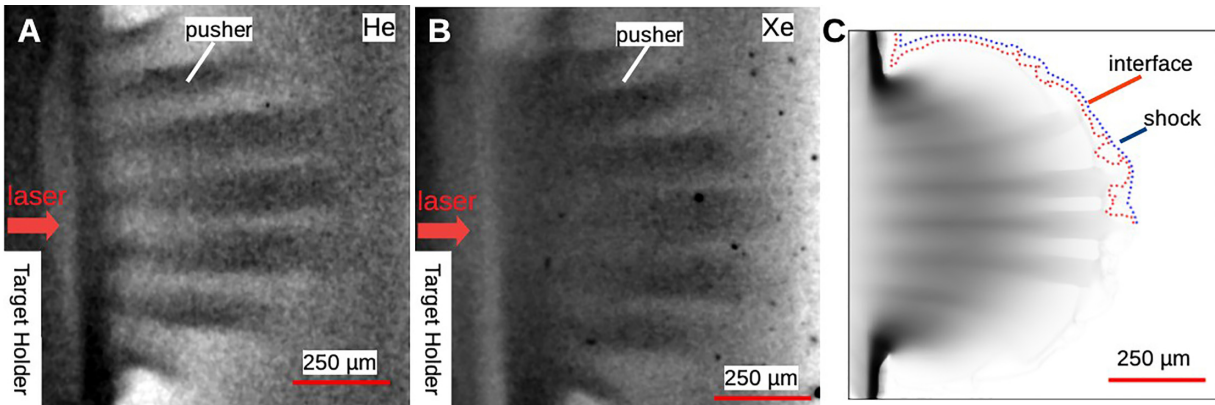


**FIG. 6.** Experimental radiographies (LULI2000) of the helium (a) and xenon (b) taken 20 ns after laser shot. Both x-ray images show the density variation inside the pusher. (c) Synthetic radiography obtained by post-processing simulations from FLASH taken 20 ns after laser shot in the xenon. The blue and red dotted lines show the respective positions of the shock and the interface, which cannot be observed due to the low density.

simulations (c). On the radiographies, the pusher appears darker than the gas since it is denser and composed of material (Br), which absorbs more x rays than the gas. A modulation can be seen in the experimental images for both He and Xe cases. However, contrary to what might be expected, this modulation does not correspond to the interface or the RTI. This is apparent with the synthetic radiography (C), where similar absorption morphology is recreated inside the pusher. According to this simulation, the actual interface and the shock have low absorption and are situated ahead of these modulations. We displayed a part of their respective position in Fig. 6(c) with dotted lines. From this comparison, we conclude that the contrast is insufficient to observe the interface and shock on the experimental x-ray images given the actual background noise and the sensitivity of our diagnostic. What we actually observe are the density modulations inside the pusher. These modulations are the results of the passage of the shock at the interface between the pusher and the gas and of the rarefaction wave going back into the pusher. In that sense, they are good indications of the development of the instabilities but are not a direct observation of the instabilities.

A difference, between the He and Xe cases, can be observed in these internal modulations. This difference pertains to the extension of the low-density bands (light) that span until the base of the pusher in the He case but are confined to its extremity with Xe. The same phenomenon is observed in our simulations. We do not explain the origin

of this difference, since the global dynamic of the pusher in Xe and He is almost the same in the low velocity (LULI2000) experiment. The only possibilities are either linked to radiative effects or the impact of the gas on the radiography. We expect only a weak impact of the RS on the internal structure as the radiations should be absorbed on the outer layer of the pusher. Here, the nature of the gas might play a greater role. Since the expanding pusher is surrounded by gas, the absorption of the x rays by this gas also impacts the radiography. Given the x-ray energy of the backlight source (4.5 keV), the attenuation cross section should be higher by a factor of  $\sim 2.6$  in Xe in comparison to He. Due to this higher absorption and the resulting drop in signal intensity, the internal modulation might not be observable in the Xe case rather than not existing or being shorter.

The use of optical diagnostics did not allow us to observe the internal structure of the pusher, as it is opaque to the visible light when it expands. They, nevertheless, allow us to study its external structure, mainly through its global morphology, the morphology of the shock, their relative position and interactions (see Figs. 7 and 8) and to observe the instabilities development. In Fig. 7, we guess the presence of the modulation between the part named beam and clump, as we do observe some modulation in intensity. However, we cannot distinguish the spikes in their entirety.

Here, only the simulations allow us to perform a direct study of the instabilities. These simulations predict a slightly quicker instability

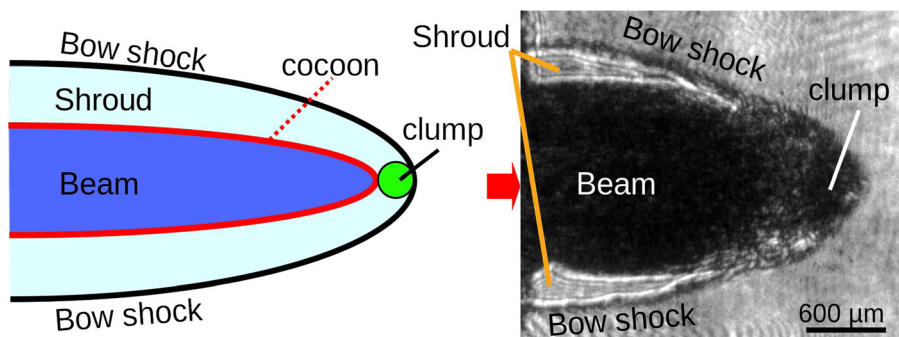


**FIG. 7.** Comparison of the experimental results to a schematic representation of radiative cooling astrophysical jets. The experimental image is a visible shadowgraphy obtained 25 ns after laser shot in He on GEKKO XII. The global structure of our shadowgraphy is similar to the schematic representation of a radiative cooling astrophysical jet according to Ref. 4.



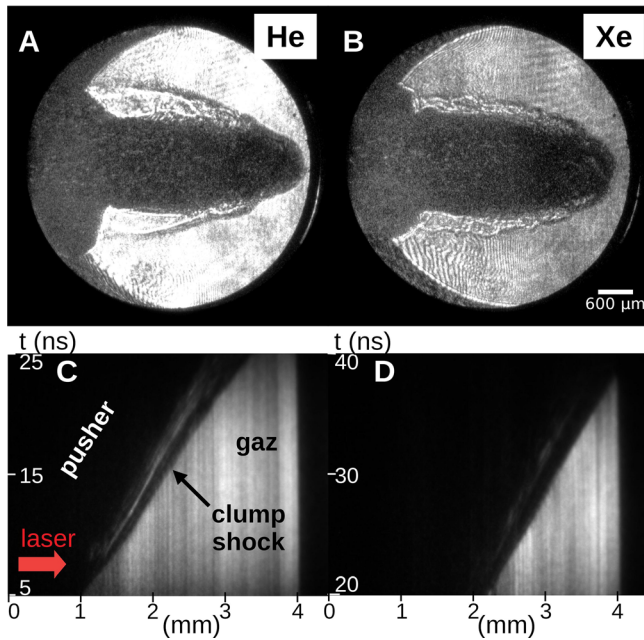


**FIG. 8.** Comparison of the jet morphology between helium (a) and (c) and xenon (b) and (d) cases. The experimental visible shadowgraphs (a) and (b) were obtained 40 ns after laser shot on GEKKO XII. The experimental visible streaked shadowgraphs (c) and (d) show the presence of the clump detached from the pusher/beam.

growth in the He case, as well as a difference in morphology with thinner spikes in He. This quicker growth in the He case might appear as surprising as the interface as a higher deceleration in Xe in our simulations. So the hydrodynamic instabilities have a slower growth in the presence of a radiative shock. This lower growth is either directly due to the radiative flux, which stabilizes the interface by lowering the RMI and RTI growth, or indirectly as the distance between shock and spikes is lower in Xe ( $\sim 5$  vs  $\sim 10 \mu\text{m}$  after 16 ns). However, we cannot be certain of such results, as our experimental results do not allow us to make such direct observations.

**IV. DISCUSSION ON THE JET MORPHOLOGY**

An interesting result of our experiment is related to the global morphology of the plasma and the shock, which we observed with our optical diagnostics. Figure 7 shows shadowgraphy result of the expansion of the plasma and the shock forming a jet into He (25 ns after laser shot). This structure can be broken down into: a plasma flow, usually called “beam,” a clump, the surrounding shocked gas making a shroud, and a bow shock. The beam is composed of pusher material and appears opaque. The clump is a heap of matter detached from the main beam. From its high opacity, one can deduce that it is either composed of matter torn from the pusher, or of highly compressed and ionized gas. The blurry zone between the beam and clump presents a regular structure. This is the zone where the instabilities are developing, and as previously reported, we associate this structure with the instability. However, the lack of observable details due to an insufficient resolution does not allow us to conclude with certainty on the real nature of this structure. The shock stays attached to the clump

at the front. However, it is detached from the beam in the lateral direction, thus forming a clear bow shock. The medium between the bow shock and the beam appears homogeneous and transparent to visible light. It is composed of shocked gas.

The global morphology of this jet reminds us of the one of astrophysical jets as described by Blondin *et al.*<sup>4</sup> Our experiment was not designed to be similar to astrophysical jets in a laboratory astrophysical way.<sup>39</sup> As such it is not surprising if the dimensionless numbers describing our system do not match exactly those of astrophysical jets. Based on Ref. 4 and references therein, in astrophysics, the density ratio of surrounding gas and beam is between 0.01 and 10, and the Mach number is usually high  $\sim 20$  even if low Mach numbers (1.2) are also studied in astrophysics. Based on our initial parameters and our simulations, in our experiments the density ratio starts at  $4 \times 10^{-5}$  and ends at  $\sim 0.04$  (40 ns Xe), and the Mach number is  $\sim 12$  (LULI2000) and  $\sim 16$  (GEKKO XII) in Xe. One might argue that our values are close enough to the astrophysical ones to claim to be in the similar category of laboratory astrophysics. However, the increase in density ratio in experiments, due to the pusher expansion and dilution, is too important to be compared to classical astrophysical jets studies, where material inflow in the jets compensates for their expansion.

Based on the morphology of astrophysical jets, there should be a cocoon surrounding the beam, typically composed of shocked beam material. It surrounds the beam and streams down it along its outer layer. In our optical observations, the beam appears opaque, and it is not surprising that we cannot distinguish the cocoon from it. This is due to their sheer proximity and to the fact that the shocked beam material, composing the cocoon, should also be opaque. One might argue that we can see the cocoon in Fig. 8(a). Indeed, the border between the opaque beam and clear shroud, in the lateral direction, seems composed of two parallel interfaces with little blurry space in between. This blurry space and second interface can correspond to the cocoon, or a boundary effect taking place in the shroud. In such a case, it would be a turbulent boundary layer composed of gas material (the viscosity induced boundary layer).

In the context of a comparison to astrophysical jets, questions arise concerning the nature of the clump preceding the beam. Since, in our experiment, this structure arises from the development of the instabilities and possibly of an accumulation of shocked gas confined by the instabilities, it could be specific to our conditions and be absent in astrophysics. However, we cannot rule out the development of similar instabilities at the front end of an astrophysical jet, since the right conditions are present (gradient of density and slight deceleration of the jet). The question would then be the size of this structure in astrophysics and its importance for the global evolution of the jet. To this question, which we will not answer, we should add a consideration concerning the front structure of the jet. Following Ref. 4, the front end of the jet becomes unstable, and different structures are formed depending on the exact conditions. These structures differ in their morphology, but they are similar in the sense that they correspond to an accumulation of material leading to a high density. In that sense, this structure is similar to our clump despite not being related to either RTI or RMI.

There are, actually, differences in morphology between the Xe and the He cases (see Fig. 8): in the distance between clump and beam, and the width and aspect of the shroud. In Xe, the clump is barely detached from the beam compared to the He case. This can be seen



both in the 2D shadowgraphies (a) and (b) and in the 1D streaked shadowgraphies (c) and (d), which show the temporal evolution in only one spatial dimension. In particular, with the streaked diagnostic, we can observe the formation and growth of the gap between the opaque pusher, which correspond to the beam, and the clump ahead of it. This gap, which corresponds to the blurry zone in the 2D images, is smaller in the xenon, pointing out that the instabilities are not well-developed. This observation is in agreement with our FLASH4 simulations, which also show a quicker instability growth in He. Theoretically, two hypotheses may explain this phenomenon. Either the radiation of the shock has a negative impact on the instability growth or the shock is too close to the interface to allow the spikes to grow.<sup>24</sup> The second explanation is an indirect consequence of the radiation. A radiative shock (Xe) loses energy and decelerates. As a consequence, the radiative shock is closer to the beam than in the non-radiative one (He). The greater proximity between a shock and interface leads to lower growth of the instabilities since it results in a higher pressure, which opposes the instabilities' development. In that sense, it is difficult to conclude the exact reason for the lower instability growth: is it directly or indirectly due to the radiation.

Baring all consideration on the effects of the radiations and the interface-shock proximity on the growth of the instabilities, the result comes as surprising. Indeed, if we consider all parameters that classically change the growth rate of RTI and RMI (the Atwood number, the wavelength of the perturbation, the interface velocity, and acceleration), we would conclude on the same growth rate for both cases, Xe and He. The only difference that might exist would be a higher RTI growth rate in the Xe case due to the slightly higher deceleration of the interface.

Concerning the shroud [Figs. 8(a) and 8(b)], it is narrower and blurrier in the xenon as compared to helium gas. This blurry aspect is the result of the loss of cylindrical symmetry of the bow shock and the inhomogeneities in the shocked Xe. As radiative losses are important in Xe, the internal energy maintaining the bow shock and shroud drop, resulting in a smaller shriveled shroud. Such a difference also exists in astrophysics between adiabatic and radiative cooling jets,<sup>4</sup> which demonstrates the relevance of our results to the astrophysical case. Other details of the morphology of the jet can be highlighted in our experiments such as the single or multiple lobes at its front depending on the nature of the gas.

## V. CONCLUSION

In conclusion, we have performed experiments on the growth of RTI and RMI in the presence of a radiative shock. While the radiations, produced by such a shock, tend to decrease the growth rate of both instabilities, the higher deceleration, due to radiative loss, enhances the RTI growth. Despite the absence of direct observations of the instability, we conclude from our indirect observation that a radiative shock leads to a lower instability growth. This conclusion is corroborated by our simulations. We interpret this decrease in growth rate as a direct consequence of the radiation, which leads to a lower gradient of density (interface ablation). However, this might also come as a result of a modification of the pressure gradient around the interface, both due to the presence of a radiative flux and the proximity of the shock, which decelerates.

The jets produced during our experiments can be compared to astrophysical radiative cooling jets. They present a clump, which

precedes the beam of matter. The importance of this clump, whose existence is related to the instabilities, is still to be determined in astrophysics.<sup>40</sup> Future experiments envisioned at MJ scale laser facilities will address this question.

## ACKNOWLEDGMENTS

We would like to acknowledge the support of the GEKKO XII laser and LULI2000 operation crews. We acknowledge also the support of C. Spindloe (Scitech Precision Ltd.) for the fabrication of the modulated pushers. This work was partially funded by the Agence Nationale de la Recherche project TurboHEDP (Project No. ANR-15-CE30-0011). This work was financially supported by the "PHC Sakura" program (Project No. 34132RE) implemented by the French Ministry of Foreign Affairs, the French Ministry of Higher Education and Research, and the Japan Society for Promotion of Science. It was also financially supported by COST (European COoperation in Science and Technology), action MP1208, with a Short-Term Scientific Mission (STMS).

## AUTHOR DECLARATIONS

### Conflict of Interest

The authors have no conflicts to disclose.

### Author Contributions

**Gabriel Rigon:** Conceptualization (equal); Data curation (equal); Formal analysis (equal); Investigation (equal); Visualization (equal); Writing – original draft (equal); Writing – review and editing (equal). **Youichi Sakawa:** Investigation (equal). **Takayoshi Sano:** Investigation (equal). **Hiroshi Shimogawara:** Investigation (supporting). **S. Tamatani:** Investigation (supporting). **Alexis Casner:** Conceptualization (equal); Funding acquisition (equal); Project administration (equal); Writing – review and editing (supporting). **Michel Koenig:** Conceptualization (equal); Funding acquisition (equal); Project administration (equal); Writing – review and editing (supporting). **Bruno Albertazzi:** Investigation (equal); Writing – review and editing (supporting). **Paul Mabey:** Investigation (equal); Writing – review and editing (supporting). **Thibault Michel:** Investigation (equal). **Patrice Barroso:** Investigation (equal). **Anatoly Yakovlevich Faenov:** Investigation (equal). **Rajesh Kumar:** Investigation (supporting). **Claire Michaut:** Investigation (equal). **Tatiana Aleksandrovna Pikuz:** Investigation (supporting).

## DATA AVAILABILITY

The data that support the findings of this study are available from the corresponding author upon reasonable request.

## REFERENCES

- <sup>1</sup>R. Drake, *High-Energy-Density Physics: Fundamentals, Inertial Fusion, and Experimental Astrophysics* (Springer, 2006).
- <sup>2</sup>Y. Zel'dovich and Y. Raizer, *Physics of Shock Waves and High-Temperature Hydrodynamic Phenomena* (Academic Press, 1967).
- <sup>3</sup>T. Michel, B. Albertazzi, P. Mabey, G. Rigon, F. Lefevre, L. Van Box Som, P. Barroso, S. Egashira, R. Kumar, C. Michaut, M. Ota, N. Ozaki, Y. Sakawa, T. Sano, E. Falize, and M. Koenig, "Laboratory observation of radiative shock deceleration and application to SN 1987A," *Astrophys. J.* **888**, 25 (2019).

- <sup>4</sup>J. M. Blondin, B. A. Fryxell, and A. Konigl, "The structure and evolution of radiatively cooling jets," *Astrophys. J.* **360**, 370 (1990).
- <sup>5</sup>E. Falize, B. Loupias, A. Ravasio, C. D. Gregory, A. Dizièrè, M. Koenig, C. Michaut, C. Cavet, P. Barroso, J.-P. Leidinger, X. Ribeyre, J. Breil, H. Takabe, Y. Sakawa, Y. Kuramitsu, T. Morita, N. C. Woolsey, W. Nazarov, and S. Pikuz, "The scalability of the accretion column in magnetic cataclysmic variables: The polar project," *Astrophys. Space Sci.* **336**, 81–85 (2011).
- <sup>6</sup>E. Falize, A. Ravasio, B. Loupias, A. Dizièrè, C. Gregory, C. Michaut, C. Busschaert, C. Cavet, and M. Koenig, "High-energy density laboratory astrophysics studies of accretion shocks in magnetic cataclysmic variables," *High Energy Density Phys.* **8**, 1–4 (2012).
- <sup>7</sup>P. Mabey, B. Albertazzi, E. Falize, T. Michel, G. Rigon, L. Van Box Som, A. Pelka, F.-E. Brack, F. Kroll, E. Filippov, G. Gregori, Y. Kuramitsu, D. Q. Lamb, C. Li, N. Ozaki, S. Pikuz, Y. Sakawa, P. Tzeferacos, and M. Koenig, "Laboratory study of stationary accretion shock relevant to astrophysical systems," *Sci. Rep.* **9**, 8157 (2019).
- <sup>8</sup>B. Fryxell, E. Mueller, and D. Arnett, "Instability and clumping in SN 1987A," *Astron. Astrophys.* **251**, 505 (1991).
- <sup>9</sup>B. E. K. Sugerman, A. P. S. Crotts, W. E. Kunkel, S. R. Heathcote, and S. S. Lawrence, "The three-dimensional circumstellar environment of SN 1987A," *Astrophys. J. Suppl. Ser.* **159**, 60–99 (2005).
- <sup>10</sup>A. Pak, L. Divol, G. Gregori, S. Weber, J. Atherton, R. Benedetti, D. K. Bradley, D. Callahan, D. T. Casey, E. Dewald, T. Döppner, M. J. Edwards, J. A. Frenje, S. Glenn, G. P. Grim, D. Hicks, W. W. Hsing, N. Izumi, O. S. Jones, M. G. Johnson, S. F. Khan, J. D. Kilkenny, J. L. Kline, G. A. Kyrala, J. Lindl, O. L. Landen, S. L. Pape, T. Ma, A. MacPhee, B. J. MacGowan, A. J. MacKinnon, L. Masse, N. B. Meezan, J. D. Moody, R. E. Olson, J. E. Ralph, H. F. Robey, H.-S. Park, B. A. Remington, J. S. Ross, R. Tommasini, R. P. J. Town, V. Smalyuk, S. H. Glenzer, and E. I. Moses, "Radiative shocks produced from spherical cryogenic implosions at the national ignition facility," *Phys. Plasmas* **20**, 056315 (2013).
- <sup>11</sup>Y. Zhou, "Rayleigh–Taylor and Richtmyer–Meshkov instability induced flow, turbulence, and mixing. I," *Phys. Rep.* **720–722**, 1–136 (2017).
- <sup>12</sup>Y. Zhou, "Rayleigh–Taylor and Richtmyer–Meshkov instability induced flow, turbulence, and mixing. II," *Phys. Rep.* **723–725**, 1–160 (2017).
- <sup>13</sup>H. Takabe, K. Mima, L. Montierth, and R. L. Morse, "Self-consistent growth rate of the Rayleigh–Taylor instability in an ablatively accelerating plasma," *Phys. Fluids* **28**, 3676–3682 (1985).
- <sup>14</sup>V. A. Smalyuk, H. F. Robey, C. L. Alday, P. Amendt, C. Aracne-Ruddle, J. R. Bigelow, T. Bunn, D. T. Casey, K.-C. Chen, D. S. Clark, J. P. Cortez, J. Crippen, S. Diaz, M. Farrell, S. Felker, J. E. Field, J. Jaquez, S. Johnson, S. W. Haan, B. A. Hammel, A. V. Hamza, M. O. Havre, C. Heinbockel, W. W. Hsing, K. Kangas, J. J. Kroll, S. O. Kucheyev, O. L. Landen, X. Lepro-Chavez, A. G. MacPhee, D. A. Martinez, J. Milovich, A. Nikroo, L. A. Pickworth, N. Rice, M. Stadermann, D. Steich, and C. R. Weber, "Review of hydro-instability experiments with alternate capsule supports in indirect-drive implosions on the national ignition facility," *Phys. Plasmas* **25**, 072705 (2018).
- <sup>15</sup>V. A. Smalyuk, C. R. Weber, O. L. Landen, S. Ali, B. Bachmann, P. M. Celliers, E. L. Dewald, A. Fernandez, B. A. Hammel, G. Hall, A. G. MacPhee, L. Pickworth, H. F. Robey, N. Alfonso, K. L. Baker, L. F. B. Hopkins, L. Carlson, D. T. Casey, D. S. Clark, J. Crippen, L. Divol, T. Döppner, M. J. Edwards, M. Farrell, S. Felker, J. E. Field, S. W. Haan, A. V. Hamza, M. Havre, M. C. Herrmann, W. W. Hsing, S. Khan, J. Kline, J. J. Kroll, S. LePape, E. Loomis, B. J. MacGowan, D. Martinez, L. Masse, M. Mauldin, J. L. Milovich, A. S. Moore, A. Nikroo, A. Pak, P. K. Patel, J. L. Peterson, K. Raman, B. A. Remington, N. Rice, M. Schoff, and M. Stadermann, "Review of hydrodynamic instability experiments in inertially confined fusion implosions on national ignition facility," *Plasma Phys. Controlled Fusion* **62**, 014007 (2019).
- <sup>16</sup>A. Casner, C. Mailliet, G. Rigon, S. Khan, D. Martinez, B. Albertazzi, T. Michel, T. Sano, Y. Sakawa, P. Tzeferacos, D. Lamb, S. Liberatore, N. Izumi, D. Kalantar, P. D. Nicola, J. D. Nicola, E. L. Bel, I. Igumenshchev, V. Tikhonchuk, B. Remington, J. Ballet, E. Falize, L. Masse, V. Smalyuk, and M. Koenig, "From ICF to laboratory astrophysics: Ablative and classical Rayleigh–Taylor instability experiments in turbulent-like regimes," *Nucl. Fusion* **59**, 032002 (2018).
- <sup>17</sup>A. Casner, L. Masse, S. Liberatore, P. Loiseau, P. E. Masson-Laborde, L. Jacquet, D. Martinez, A. S. Moore, R. Seugling, S. Felker, S. W. Haan, B. A. Remington, V. A. Smalyuk, M. Farrell, E. Giraldez, and A. Nikroo, "Probing the deep nonlinear stage of the ablative Rayleigh–Taylor instability in indirect drive experiments on the national ignition facility," *Phys. Plasmas* **22**, 056302 (2015).
- <sup>18</sup>A. Casner, L. Masse, B. Delorme, D. Martinez, G. Huser, D. Galmiche, S. Liberatore, I. Igumenshchev, M. Olazabal-Loumé, P. Nicolaï, J. Breil, D. T. Michel, D. Froula, W. Seka, G. Riazuelo, S. Fujioka, A. Sunahara, M. Grech, C. Chicanne, M. Theobald, N. Borisenko, A. Orekhov, V. T. Tikhonchuk, B. Remington, V. N. Goncharov, and V. A. Smalyuk, "Progress in indirect and direct-drive planar experiments on hydrodynamic instabilities at the ablation front," *Phys. Plasmas* **21**, 122702 (2014).
- <sup>19</sup>D. S. Clark and M. Tabak, "Nonlinear Rayleigh–Taylor growth in converging geometry," *Phys. Rev. E* **71**, 055302 (2005).
- <sup>20</sup>J. Sanz, "Self-consistent analytical model of the Rayleigh–Taylor instability in inertial confinement fusion," *Phys. Rev. E* **53**, 4026 (1996).
- <sup>21</sup>R. Betti and J. Sanz, "Bubble acceleration in the ablative Rayleigh–Taylor instability," *Phys. Rev. Lett.* **97**, 205002 (2006).
- <sup>22</sup>C. C. Kuranz, H.-S. Park, C. M. Huntington, A. R. Miles, B. A. Remington, T. Plewa, M. R. Trantham, H. F. Robey, D. Shvarts, A. Shimony, K. Raman, S. Maclaren, W. C. Wan, F. W. Doss, J. Kline, K. A. Flippo, G. Malamud, T. A. Handy, S. Prisbrey, C. M. Krauland, S. R. Klein, E. C. Harding, R. Wallace, M. J. Grosskopf, D. C. Marion, D. Kalantar, E. Giraldez, and R. P. Drake, "How high energy fluxes may affect Rayleigh–Taylor instability growth in young supernova remnants," *Nat. Commun.* **9**, 1564 (2018).
- <sup>23</sup>B. A. Remington, H.-S. Park, D. T. Casey, R. M. Cavallo, D. S. Clark, C. M. Huntington, C. C. Kuranz, A. R. Miles, S. R. Nagel, K. S. Raman, and V. A. Smalyuk, "Rayleigh–Taylor instabilities in high-energy density settings on the national ignition facility," *Proc. Natl. Acad. Sci.* **116**, 18233–18238 (2019).
- <sup>24</sup>S. G. Glendinning, J. Bolstad, D. Braun, M. Edwards, W. Hsing, B. Lasinski, H. Louis, A. Miles, J. Moreno, T. Peyser *et al.*, "Effect of shock proximity on Richtmyer–Meshkov growth," *Phys. Plasmas* **10**, 1931–1936 (2003).
- <sup>25</sup>G. Rigon, B. Albertazzi, P. Mabey, T. Michel, E. Falize, V. Bouffetier, L. Ceurvorst, L. Masse, M. Koenig, and A. Casner, "Exploring the Atwood-number dependence of the highly nonlinear Rayleigh–Taylor instability regime in high-energy-density conditions," *Phys. Rev. E* **104**, 045213 (2021).
- <sup>26</sup>S. Bouquet, C. Stehlé, M. Koenig, J.-P. Chièze, A. Benuzzi-Mounaix, D. Batani, S. Leygnac, X. Fleury, H. Merdji, C. Michaut, F. Thais, N. Grandjouan, T. Hall, E. Henry, V. Malka, and J.-P. J. Lafon, "Observations of laser driven supercritical radiative shock precursors," *Phys. Rev. Lett.* **92**, 225001–225004 (2004).
- <sup>27</sup>B. A. Remington, R. P. Drake, and D. D. Ryutov, "Experimental astrophysics with high power lasers and Z pinches," *Rev. Mod. Phys.* **78**, 755–807 (2006).
- <sup>28</sup>A. Reighard, R. Drake, K. Dannenberg, D. Kremer, M. Grosskopf, E. Harding, D. Leibbrandt, S. Glendinning, T. Perry, B. Remington *et al.*, "Observation of collapsing radiative shocks in laboratory experiments," *Phys. Plasmas* **13**, 082901 (2006).
- <sup>29</sup>M. Koenig, T. Michel, R. Yurchak, C. Michaut, B. Albertazzi, S. Laffite, E. Falize, L. V. B. Som, Y. Sakawa, T. Sano, Y. Hara, T. Morita, Y. Kuramitsu, P. Barroso, A. Pelka, G. Gregori, R. Kodama, N. Ozaki, D. Lamb, and P. Tzeferacos, "Interaction of a highly radiative shock with a solid obstacle," *Phys. Plasmas* **24**, 082707 (2017).
- <sup>30</sup>F. Suzuki-Vidal, T. Clayson, C. Stehlé, G. F. Swadling, J. M. Foster, J. Skidmore, P. Graham, G. C. Burdiak, S. V. Lebedev, U. Chaulagain, R. L. Singh, E. T. Gumbrell, S. Patankar, C. Spindloe, J. Larour, M. Kozlova, R. Rodriguez, J. M. Gil, G. Espinosa, P. Velarde, and C. Danson, "Counterpropagating radiative shock experiments on the orion laser," *Phys. Rev. Lett.* **119**, 055001 (2017).
- <sup>31</sup>G. Rigon, A. Casner, B. Albertazzi, T. Michel, P. Mabey, E. Falize, J. Ballet, L. Van Box Som, S. Pikuz, Y. Sakawa, T. Sano, A. Faenov, T. Pikuz, N. Ozaki, Y. Kuramitsu, M. P. Valdivia, P. Tzeferacos, D. Lamb, and M. Koenig, "Rayleigh–Taylor instability experiments on the LULI2000 laser in scaled conditions for young supernova remnants," *Phys. Rev. E* **100**, 021201 (2019).
- <sup>32</sup>P. Mora, "Theoretical model of absorption of laser light by a plasma," *Phys. Fluids* **25**, 1051–1056 (1982).
- <sup>33</sup>R. Fabbro, C. Max, and E. Fabre, "Planar laser-driven ablation: Effect of inhibited electron thermal conduction," *Phys. Fluids* **28**, 1463–1481 (1985).
- <sup>34</sup>D. E. Fratanduono, T. R. Boehly, P. M. Celliers, M. A. Barrios, J. H. Eggert, R. F. Smith, D. G. Hicks, G. W. Collins, and D. D. Meyerhofer, "The direct measurement of ablation pressure driven by 351-nm laser radiation," *J. Appl. Phys.* **110**, 073110 (2011).

- <sup>35</sup>P. Mabey, T. Michel, B. Albertazzi, E. Falize, N. Charpentier, and M. Koenig, "Calculating the temperature of strongly radiative shocks," *Phys. Plasmas* **27**, 083302 (2020).
- <sup>36</sup>P. Tzeferacos, A. Rigby, A. F. A. Bott, A. R. Bell, R. Bingham, A. Casner, F. Cattaneo, E. M. Churazov, J. Emig, F. Fiuza, C. B. Forest, J. Foster, C. Graziani, J. Katz, M. Koenig, C.-K. Li, J. Meinecke, R. Petrasso, H.-S. Park, B. A. Remington, J. S. Ross, D. Ryu, D. Ryutov, T. G. White, B. Reville, F. Miniati, A. A. Schekochihin, D. Q. Lamb, D. H. Froula, and G. Gregori, "Laboratory evidence of dynamo amplification of magnetic fields in a turbulent plasma," *Nat. Commun.* **9**, 591 (2018).
- <sup>37</sup>B. Fryxell, K. Olson, P. Ricker, F. X. Timmes, M. Zingale, D. Q. Lamb, P. MacNeice, R. Rosner, J. W. Truran, and H. Tufo, "FLASH: An adaptive mesh hydrodynamics code for modeling astrophysical thermonuclear flashes," *Astrophys. J. Suppl.* **131**, 273–334 (2000).
- <sup>38</sup>A. Dubey, A. Almgren, J. Bell, M. Berzins, S. Brandt, G. Bryan, P. Colella, D. Graves, M. Lijewski, F. Löffler, B. O'Shea, E. Schnetter, B. Van Straalen, and K. Weide, "A survey of high level frameworks in block-structured adaptive mesh refinement packages," *J. Parallel Distrib. Comput.* **74**, 3217–3227 (2014).
- <sup>39</sup>D. Ryutov, R. P. Drake, J. Kane, E. Liang, B. A. Remington, and W. M. Wood-Vasey, "Similarity criteria for the laboratory simulation of supernova hydrodynamics," *Astrophys. J.* **518**, 821–823 (1999).
- <sup>40</sup>B. Balick, M. Huarte-Espinosa, A. Frank, T. Gomez, J. Alcolea, R. L. Corradi, and D. Vinković, "Outflows from evolved stars: The rapidly changing fingers of CRL 618," *Astrophys. J.* **772**, 20 (2013).